Int. J. Electrochem. Sci., 15 **(2020)** 966 – 976, doi; 10.20964/2020.01.55

International Journal of
ELECTROCHEMICAL
SCIENCE
www.electrochemsci.org

Triangular Prism Shaped Co_3O_4 as a high-performance Electrode Material for Supercapacitors

Hongmei Chen[1], *Chenyang Xue*[1,*], *Danfeng Cui*[1], *Yuankai Li*[1], *Yueqing Wang*[2], *Wendong Zhang*[1,*]

[1] Science and Technology on Electronic Test and Measurement Laboratory, North University of China, Taiyuan, Shanxi 030051, China
[2] School of Energy and Power Engineering, North University of China, Taiyuan, Shanxi 030051, China
[*]E-mail: Xuechenyang@nuc.edu.cn, wdzhang@nuc.edu.cn

Received: 30 September 2019 / *Accepted:* 4 November 2019 / *Published:* 30 November 2019

Herein, triangular prism shaped Co_3O_4 material was constructed by a facile route and used as a supercapacitor electrode. The Co_3O_4 material was fully characterized by X-ray diffraction (XRD), Fourier transform infrared spectroscopy (FTIR), X-ray photoelectron spectroscopy (XPS), scanning electron microscope (SEM) and transmission electron microscope (TEM). Electrochemical characterization revealed that the Co_3O_4 material showed a high specific capacitance of 907.1 F g^{-1} at a current density of 1A g^{-1} and excellent cycle stability (with 86.5% of the initial specific capacitance remaining after 3000 cycles) at a current density of 10 A g^{-1}. Additionally, an energy density of 23.0 Wh/kg with a power density of 0.26 kW/kg was obtained over the Co_3O_4.

Keywords: Co_3O_4; electrochemical; supercapacitors; energy density

1. INTRODUCTION

Although the utilization of non-renewable fossil fuels has promoted industrial development, environmental pollution caused by the burning of fossil fuels has become increasingly serious. Thus, the development of renewable clean energy and high-performance energy storage devices is an urgent challenge [1]. Among many energy storage devices, supercapacitors have attracted increasing attention due to their advantages, including their high power density, high specific capacity and good cycle stability [2-4]. The performance of supercapacitors has been frequently investigated [5-7]. Various kinds of transition metal oxides, including RuO_2 [8], NiO [9-11], Co_3O_4 [12-15], $NiCo_2O_4$ [16], MnO_2 [17-20] and ZnO [21-23], have been employed as electrode materials.

Among the various electrode materials, the inexpensive material Co_3O_4 is a potential candidate for supercapacitors, since it has a high theoretical capacitance (3560 F/g) and is environmentally friendly [24-26]. Many different morphologies of Co_3O_4 have been studied using different preparation methods to improve its electrochemical properties. For example, hierarchical Co_3O_4 films have been prepared by electrodeposition [27], nanoporous Co_3O_4 has been prepared by a solvothermal method [28], needle-like Co_3O_4 has been prepared by a hydrothermal method [29], and 3D nanonet hollow structured Co_3O_4 has been prepared by calcination [30]. Although the properties of Co_3O_4 have been improved to a certain extent, the actual application of Co_3O_4 remains limited by a low specific capacitance, poor cycle stability and poor electronic conductivity. According to previous reports, the morphology of the Co_3O_4 material significantly affects its electrochemical properties. This presents a challenge to further improve the electrochemical performance of Co_3O_4 by designing new synthesis routes that are capable of producing a uniform, suitable morphology.

Herein, a novel and facial strategy was proposed to prepare triangular prism shaped Co_3O_4. Additionally, the composition, structure and chemical properties of the Co_3O_4 were fully characterized and discussed. The electrochemical performance of the Co_3O_4 electrode material was tested in 6 M KOH as the electrolyte. The Co_3O_4 delivered a high specific capacitance of 907.1 F g^{-1} at a current density of 1 A g^{-1} and excellent cycle stability, with 86.5% of the initial specific capacitance retained after 3000 cycles at a current density of 10 A g^{-1}. Meanwhile, an energy density of 23.0 Wh/kg with a power density of 0.26 kW/kg was obtained. Therefore, this triangular prism shaped Co_3O_4 is a very promising energy storage material.

2. EXPERIMENTAL

2.1. Sample preparation

All of the reagents used in this paper were analytic reagents purchased from Sinopharm Group Co., Ltd.

In a typical preparation of the triangular prism shaped Co_3O_4, 5 mmol of $CoCl_2 \cdot 6H_2O$ was added to 100 ml of ethanol and magnetically stirred for 5 min to make it dissolve completely. Then, 15 mmol of NH_4HCO_3 was added to the solution and stirred for another 6 h at 50 °C in a thermostatic water bath. After the reaction, the obtained particles were washed with ethanol and centrifuged. The particles were subsequently dried at 70 °C for one night and calcined at 350 °C for 2 h with a heating rate of 2 °C/min.

2.2. Characterization

XRD was performed on a Bruker D8 Advance with a canning step of 0.02, a working voltage of 40kV and a working current of 30 mA. Fourier transform infrared (FTIR) spectra were obtained using a NEXUS Thermo Nicolet IR spectrometer. The Brunauer-Emmett-Teller (BET) specific surface area and pore structure were tested on a NOVA2200e instrument. Scanning electron microscopy (SEM) and transmission electron microscopy (TEM) were carried out on a Hitachi SU8220 and a FEI Tecnai G2

F20, respectively. X-ray photoelectron spectroscopy (XPS) was performed using an Escalab 250 Xi instrument.

2.3. Electrochemical measurements

All the electrochemical performance tests were performed in 6 M KOH as the electrolyte using an electrochemical workstation (RST 5000) for a three-electrode configuration with a platinum wire as the counter electrode and a saturated calomel electrode as the reference electrode. The working electrode was prepared as follows: 85% Co_3O_4, 10% acetylene black, and 5% PVDF were mixed together, then ethanol and two drops of polytetrafluoroethylene (PTFE) were added. Then the mixture was uniformly coated onto a Ni foam substrate (1 cm × 1 cm) and dried at 70 °C. Cyclic voltammetry, galvanostatic charge-discharge, and EIS measurements were carried out to evaluate the electrochemical properties of the Co_3O_4. For the two-electrode device, the electrochemical properties were tested using the prepared Co_3O_4 as the anode material and activated carbon as the cathode material in the 6 M KOH as the electrolyte.

3. RESULTS AND DISCUSSION

3.1. Sample Characterization

XRD and FTIR spectroscopy were carried out to confirm the composition of the material. As seen in Figure 1a, a series of diffraction peaks were observed, centered at 19.0°, 31.3°, 36.9°, 38.5°, 44.8°, 55.7°, 59.4°, 65.2°, 68.6°, 77.3°, 78.4°, and 82.6°, that can be attributed to the (111), (220), (311), (222), (400), (422), (511), (440), (531), (620), (533), (622) and (444) plans of Co_3O_4, consistent with PDF#42-1467 (the red line). The FTIR spectrum is presented in Figure 1b. The peaks at 667 cm^{-1} and 570 cm^{-1} can be assigned to the Co(2p)-O and Co(3p)-O stretching vibrations, respectively [31], while the peaks centered at 1624 cm^{-1} and 3385 cm^{-1} can be ascribed to the O-H stretching and bending vibrations of surface-adsorbed water [32-33]. The XRD and FTIR results reveal the phase composition of the prepared Co_3O_4.

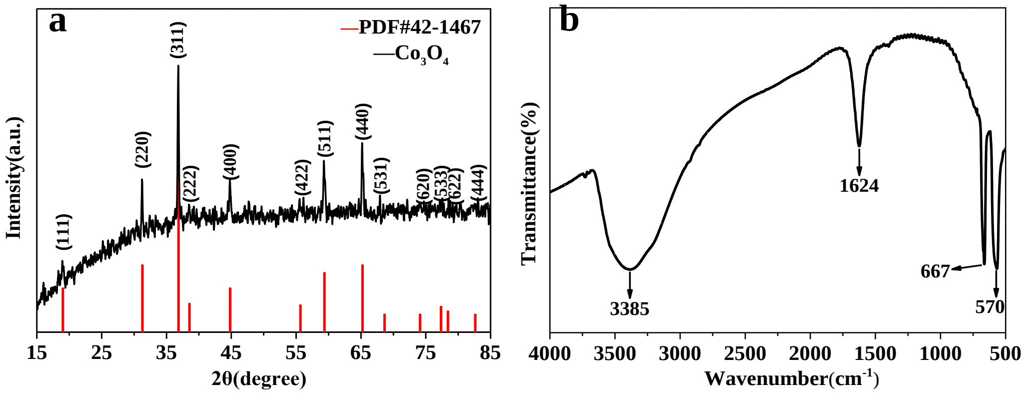

Figure 1. XRD patterns (a) and FTIR spectrum (b) of the Co_3O_4

XPS is a useful technique for analyzing the chemical states of materials using their different characteristic spectral lines. Figure 2 shows the XPS spectrum of the prepared Co_3O_4. The obvious peaks centered at 794.7 eV and 780.5 eV in Figure 2a can be assigned to the Co $2p_{2/3}$ and Co $2p_{1/3}$, respectively [34-35]. Furthermore, the strong peaks located at 781.6 eV and 797.1 eV can be attributed to Co^{2+}, while the peaks situated at 780.0 eV and 795.2 eV can be attributed to Co^{3+} after fitting the spectra using the Gaussian peak fitting method [36-37]. As shown in Figure 2b, the broad peak at 530.1 eV can be assigned to the O 1s [38]. The XPS results further confirm the successful preparation of Co_3O_4, consistent with the XRD and FTIR results.

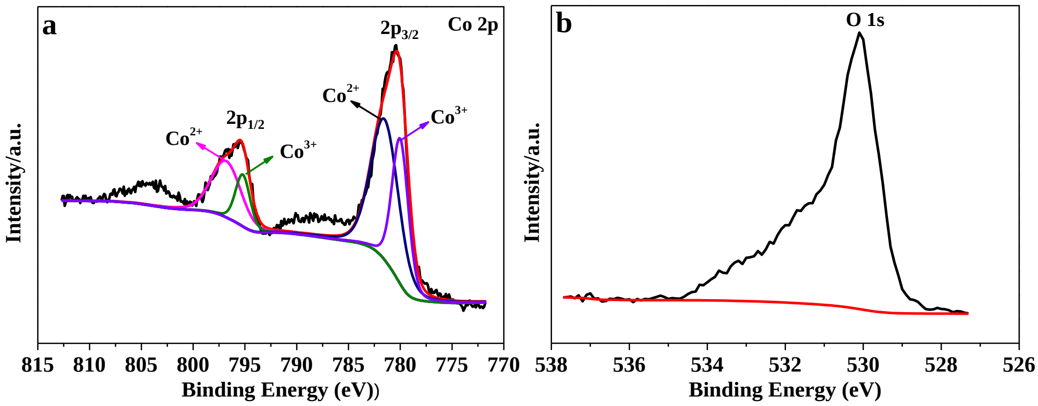

Figure 2. XPS spectrum of the Co_3O_4

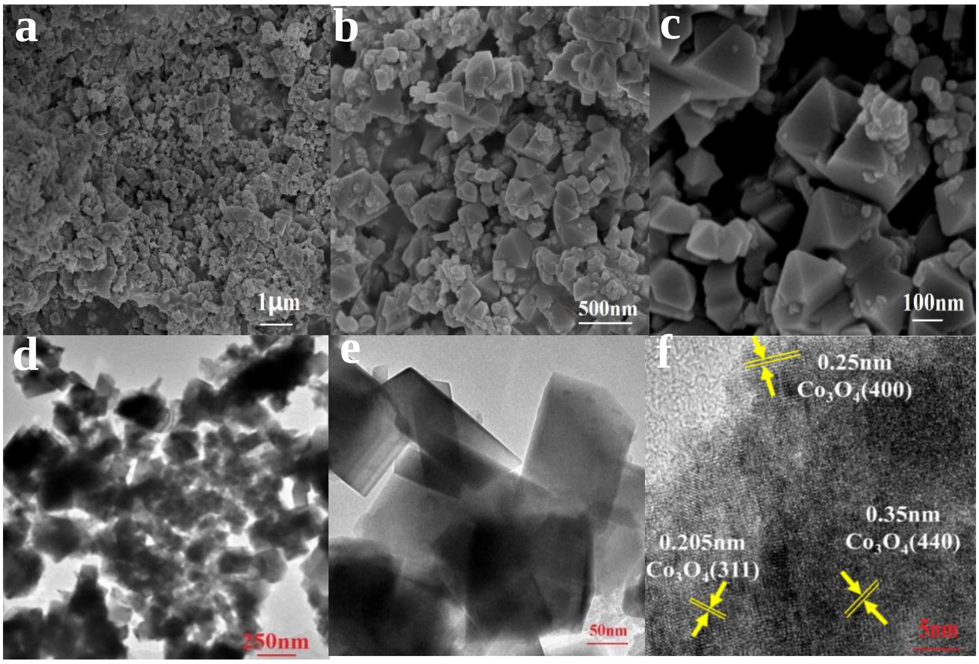

Figure 3. SEM (a-c) images, TEM (d-f) images of the Co_3O_4

In order to accurately understand the morphology and the internal structure of the Co_3O_4 material, SEM and TEM were performed. The results are shown in Figure 3. Figure 3(a-c) shows the SEM results for the prepared Co_3O_4. The structure of the nanoparticles was tight and uniform. In addition, the Co_3O_4 contained many triangular prism shaped nanoparticles. Figure 3(d-f) shows the TEM images of the Co_3O_4 nanoparticles. It can be clearly seen that the Co_3O_4 nanoparticles formed a triangular prism shape, which was similar to the images obtained from SEM. As shown in the Figure 3f, three kinds of lattice spacings, 0.25 nm, 0.205 nm and 0.35 nm were observed, consistent with the (400), (311) and (440) planes of the Co_3O_4 nanoparticles, respectively.

Figure 4 shows the microstructure of the Co_3O_4 nanoparticles, determined by N_2 adsorption-desorption analysis. The N_2 adsorption isotherms of the prepared Co_3O_4 belonged to type-IV. The specific surface area was 17.8 m^2/g and the pore volume was 0.051 cc/g.

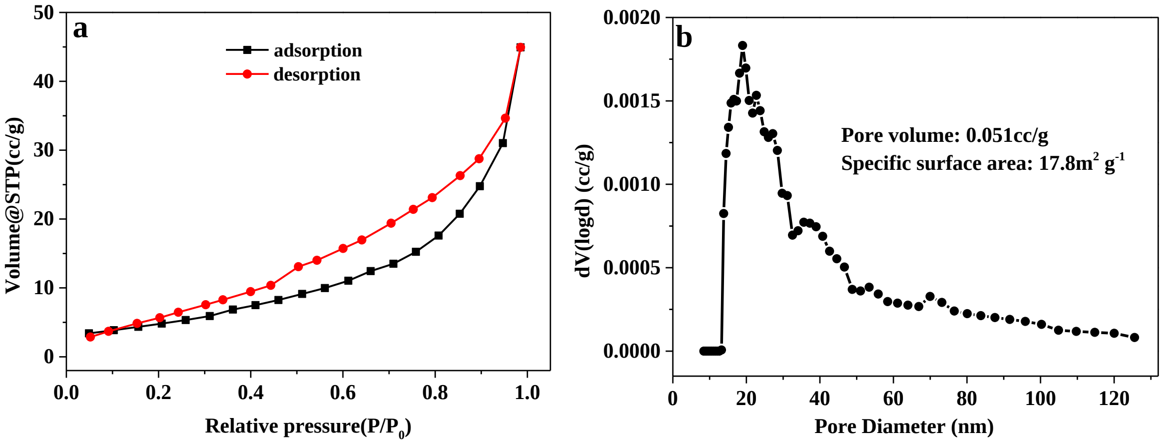

Figure 4. N_2 adsorption-desorption isotherm (a) and correspond to pore size distributions (b) of Co_3O_4 particle

3.2. Electrochemical properties

The electrochemical properties of the prepared Co_3O_4 electrode material were evaluated using a three-electrode system. Cyclic voltammetry (CV) was performed from 5 mV S^{-1} to 100 mV S^{-1}. As shown in Figure 5a, two obvious redox peaks can be observed in each CV, indicating that the Co_3O_4 shows pseudocapacitance [39]. The redox peaks moved in two directions as the scan rate increased. Additionally, the intensity of the peaks gradually decreased due to impedance and the polarization effect. Figure 5b shows the galvanostatic charge/discharge curves at different current densities. The inclination curves can be distinctly observed between 0.1 and 0.2 V, which further demonstrates the pseudocapacitance of the material. Figure 5c displays the different mass specific capacitances at different current densities obtained from the galvanostatic charge/discharge tests. The mass specific capacitances (C/F g^{-1}) were calculated using the following formula:

$$C = \frac{I\Delta t}{m_s \Delta V}$$

where I is the discharge current (in amperes), Δt is the discharge time (in seconds), m_s is the active material quality (in grams), and ΔV is the charge and discharge potential difference. The mass specific capacitances were 907.1, 825.8, 774.2, 636.3 and 593.4 F g^{-1} at current densities of 1, 2, 3, 5, 8 and 10

A g^{-1}, respectively. These results show that the mass specific capacitance retains a very good value of 593.4 F g^{-1} at a current density of 10 A g^{-1}, which is 65.4% of the initial value of 907.1 F g^{-1} at 1 A g^{-1}. In addition, the specific capacitance is superior to many results reported by previous studies (Table 1).

Table 1. Different electrochemical properties in previous reports for surpercapacitors

Material	Specific Capacitance (F g^{-1})	Current density	Capacity Retention //Cycling number	Reference
Co_3O_4	476	0.5 A g^{-1}	82%//2000	[28]
Co_3O_4	157.7	0.1 A g^{-1}	70%//4000	[29]
Co_3O_4	384.375	3 A g^{-1}	96.54%//1000	[40]
Co_3O_4	739	1 A g^{-1}	90.2%//1000	[41]
Co_3O_4-0.5/MWCNT	273	0.5 A g^{-1}	88%//500	[42]
Co_3O_4	570	2 A g^{-1}	74%//2000	[43]
Co_3O_4/Graphene	357	0.5 A g^{-1}	87%//1000	[44]
Co_3O_4 NSs-rGO	187	1.2 A g^{-1}	89%//1000	[45]
ZnO@Co_3O_4	857.7	1 A g^{-1}	78%//6000	[46]
Co_3O_4	162	2.75 A g^{-1}	72.2%//1000	[47]
Co_3O_4/r-GO	163.8	1 A g^{-1}	93%//1000	[48]
Co_3O_4	111	2.5mA cm^{-1}	88.2%//1000	[49]
Co_3O_4	235	20mV s^{-1}	Not mentioned	[50]
Co_3O_4	390.4	1 A g^{-1}	95%//500	[51]
Co_3O_4	814	1 A g^{-1}	Not mentioned	[52]
Sn-doped Co_3O_4	151.8	5 mV s^{-1}	Not mentioned	[53]
MnO_2@Co_3O_4	234	200mA g^{-1}	87.5%//2000	[54]
Co_3O_4	907.1	1 A g^{-1}	86.5%//3000	This work

In order to further evaluate the electrochemical properties of the Co_3O_4 electrode material, cycling stability tests were performed at 10 A g^{-1}. As shown in Figure 5d, the mass specific capacitance decreased gradually from 593.4 F g^{-1} to 500.4 F g^{-1} after the 400th cycle. After that, the mass specific capacitance remained stable at a value of 513.3 F g^{-1}, which is 86.5% of the initial value after 3000 cycles, indicating good cycle stability. Figure 5e and Figure 5f show the EIS curve, as well as the fitted curve and the equivalent circuit based on the fitting results. As seen in Figure 5e, the EIS curve and the fitted curve agree well and the fitting error is only 8.14×10^{-04}. The R_s, R_{ct1}, R_{ct2}, and R_{ct3} of the Co_3O_4 electrode are 0.36 Ω, 9.4 Ω, 0.06 Ω and 0.01 Ω, respectively. The low equivalent series resistance and charge transfer resistance results indicate the Co_3O_4 electrode has that excellent conductivity and a rapid charge transfer rate.

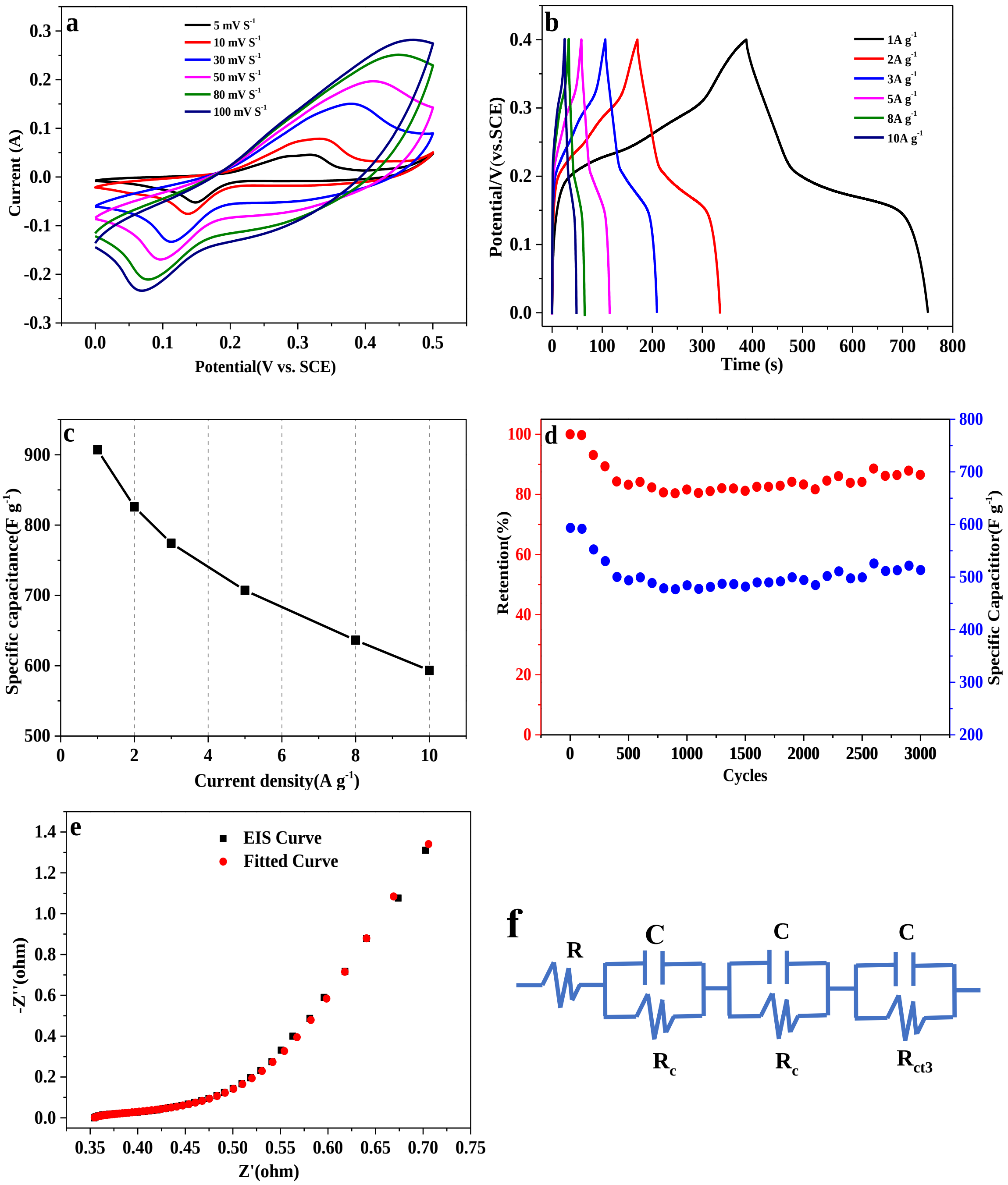

Figure 5. The electrochemical performances of the Co_3O_4 (a) CV curves; (b) galvanostatic charge/discharge curves; (c) specific capacitance at different current densities; (d) cycle stability test at 10A g^{-1}; (e) EIS test and (f) the equivalent circuit.

In order to satisfy requirements for practical application as an electrode material, the electrochemical performance of a Co_3O_4//AC two electrode system was tested. The energy density (E-Wh/kg) and power density (P-kW/kg) were obtained using the following equations [47]:

$$\mathrm{E} = \frac{C \times (\Delta V)^2}{2}$$

$$\mathrm{P} = \frac{E}{t}$$

where C is the mass capacitance (in units of F g^{-1}), V is the potential window (V), and t is the discharge time (h).

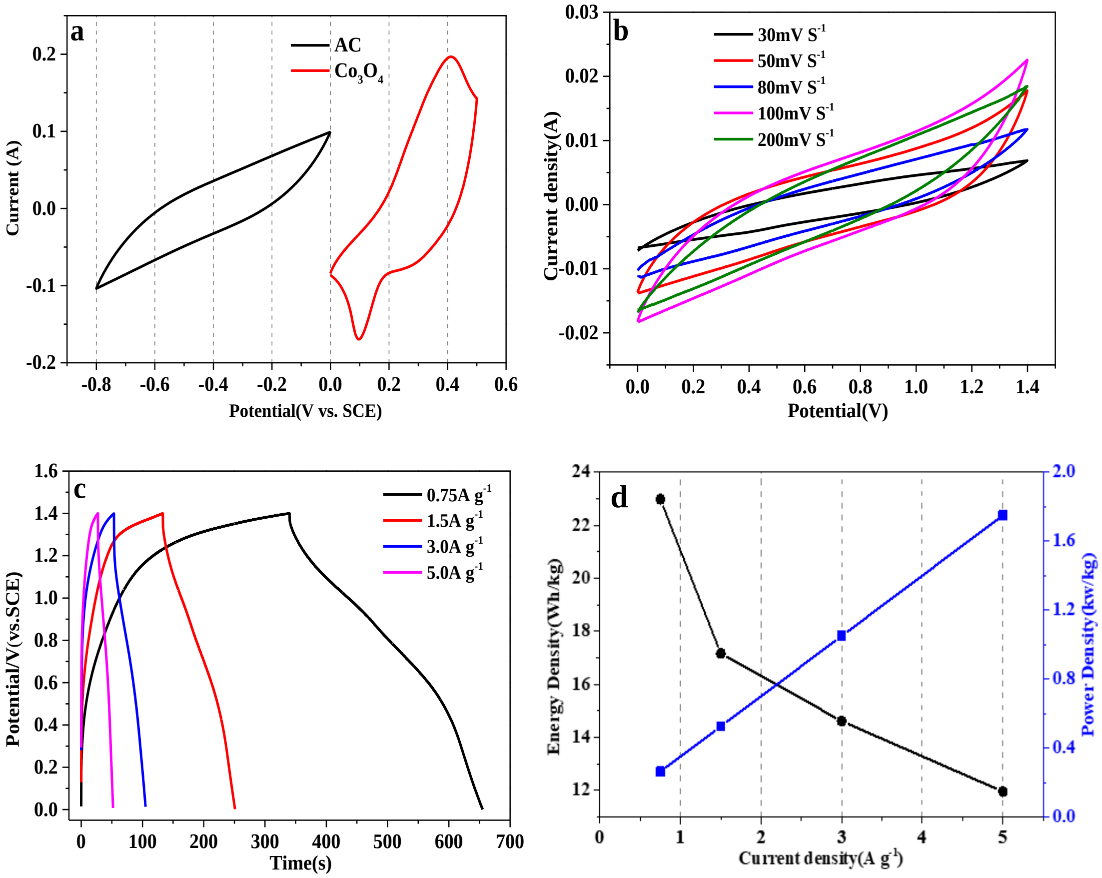

Figure 6. (a) CV curves of the Co_3O_4 electrode and the AC electrode; (b) CV and (c) galvanostatic charge-discharge curves of the Co_3O_4//AC two electrode system; (d) the energy and power densities of the Co_3O_4//AC two electrode system.

CV tests were performed for the AC electrode and the Co_3O_4 electrode. As seen in Figure 6a, the capacitance of the prepared Co_3O_4 was higher than that of AC. The CV properties of the Co_3O_4//AC two electrode system are presented in Figure 6b. The CV curves show redox peaks that decrease in intensity as the scan rate increases from 30 mV S^{-1} to 200 mV S^{-1}. In addition, the redox peaks move towards the poles because of polarization. The galvanostatic charge/discharge tests are shown in Figure 6c. The mass specific capacitances were 168.8, 126.1, 107.4 and 87.8 F g^{-1} at current densities of 0.75, 1.5, 3 and 5 A g^{-1}, respectively. Figure 6d shows the energy density and power density at different current densities for the Co_3O_4//AC two electrode system. The energy density decreased gradually as the power density increased. The highest energy density observed was 23.0 Wh/kg at a power density of 0.26 kW/kg.

4. CONCLUSIONS

In summary, triangular prism shaped Co_3O_4 was successfully synthesized via a facile method and used as an electrode material. The physicochemical properties and structures of the Co_3O_4 material were examined using various characterization methods including XRD, FTIR, XPS, SEM, TEM and BET. Furthermore, the electrochemical properties of the material were tested. The triangular prism shaped Co_3O_4 showed an excellent capacitance of 907.1 F g^{-1} at the current density of 1A g^{-1}. In addition, the Co_3O_4 delivered an excellent specific capacitance of 513.3 F g^{-1} after 3000 cycles at a current density of 10 A g^{-1}, which is about 86.5% of its initial capacitance. Also, a maximum energy density of 23.0 Wh/kg^{-1} was obtained over the Co_3O_4 at a power density of 0.26 kW/kg. Thus, this triangular prism shaped Co_3O_4 is a promising candidate for use in supercapacitors due to its excellent mass specific capacitance, energy density, and cycling stability. Additionally, the Co_3O_4 material may be useful for catalysis or sensors due to its excellent crystallinity and suitable specific surface area and pore structure.

ACKNOWLEDGMENTS
This work was supported by the School Foundation for North University of China (Grant No. 110246), Shanxi Science foundation of China(Grant No. 201801D221197), Shanxi Scholarship Council of China (Grant No. 2017-094), Shanxi Scholarship Council of China (Grant No. 2017-094), the National Science Foundation of China (Grant No.61501408), and Shanxi '1311 project' Key Subject Construction(1331KSC) for supporting this work.

References

1. P. Simon, Y. Gogotsi, *Nat. Mater.*, 7(2008)845.
2. P. Du, X. Hu, C. Yi, H.C. Liu, P. Liu, H.-L. Zhang, X. Gong, Adv. *Funct. Mater.*, 25(2015)2420.
3. R. Narayanan, P.N. Kumar, M. Deepa, A.K. Srivastava, Combining energy conversion and storage: a solar powered supercapacitor, *Electrochim. Acta*, 178(2015)113.
4. N. Goubard-Bretesché, O. Crosnier, C. Payen, F. Favier, T. Brousse, *Electrochem. Commun.*, 57(2015)61.
5. J. Jiang, Y. Li, J. Liu, X. Huang, C. Yuan, X.W. Lou, *Adv. Mater.*, 24(2012)5166.
6. B.L. Ellis, P. Knauth, T. Djenizian, *Adv. Mater.*, 26(2014)3368.
7. C. Liu, F. Li, L.-P. Ma, H.-M. Cheng, *Adv. Mater.*, 22(2010)E28.
8. V. Patake, C. Lokhande, O.S. Joo, *Appl. Surf. Sci.*, 255(2009)4192.
9. J. Li, W. Zhao, F. Huang, A. Manivannan, N. Wu, *Nanoscale*, 3(2011)5103.
10. M. Liu, J. Chang, J. Sun, L. Gao, *Electrochim. Acta*, 107(2013)9.
11. Y. Feng, H. Zhang, Y. Zhang, Y. Bai, Y. Wang, *J. Mater. Chem. A*, 4(2016)3267.
12. X. Xia, J. Tu, Y. Mai, X. Wang, C. Gu, X. Zhao, *J. Mater. Chem.*, 21(2011)9319.
13. X.Y. Liu, Y.Q. Gao, G.W. Yang, *Nanoscale*,8(2016)4227.
14. B. Wang, Y. Wang, J. Park, H. Ahn, G. Wang, *J. Alloy. Compd.*, 509(2011)7778.
15. S.K. Ujjain, G. Singh, R.K. Sharma, *Electrochim. Acta*, 169(2015)276.
16. W. Zhou, D. Kong, X. Jia, C. Ding, C. Cheng, G. Wen, *J. Mater. Chem.*, A2 (2014)6310.
17. Q. Hu, M. Tang, M. He, N. Jiang, C. Xu, D. Lin, Q. Zheng, *J. Power Sources*, 446(2020)227335.
18. X. Dong, X. Wang, J. Wang, H. Song, X. Li, L. Wang, M.B. Chan-Park, C.M. Li, P. Chen, *Carbon*, 50(2012)4865.

19. Z.-H. Huang, Y. Song, D.-Y. Feng, Z. Sun, X. Sun, X.-X. Liu, *ACS Nano.*, 12(2018)3557.
20. J. Kang, A. Hirata, L. Kang, X. Zhang, Y. Hou, L. Chen, C. Li, T. Fujita, K. Akagi, M.W. Chen, *Angew. Chem. Int. Ed.*, 52(2013)1664.
21. J. Yuan, X. Zhang, C. Chen, Y. Hao, R. Agrawal, C. Wang, W. Li, H. Yu, Y. Yu, X. Zhu, Z. Xiong, Y.M. Xie, *Mater. Lett.*, 190(2017)37.
22. H. Yue, Z. Shi, Q. Wang, Z. Cao, H. Dong, Y. Qiao, Y. Yin, S. Yang, *ACS Appl. Mater. Interfaces*, 6(2014)17067.
23. W. Liu, X. Li, M. Zhu, X. He, *J. Power Sources*, 282(2015)179.
24. X. Zheng, Z. Han, W. Yang, F. Qu, B. Liu, X. Wu, *Dalton Trans.*, 45(2016)16850.
25. J. Wang, X. Zhang, Q. Wei, H. Lv, Y. Tian, Z. Tong, X. Liu, J. Hao, H. Qu, J. Zhao, Y. Li, L. Mai, *Nano Energy*, 19(2016)222.
26. L.-F. Chen, Q. Xu, *Science*, 358(2017)304.
27. Y. Liang, Y. Li, H. Wang, J. Zhou, J. Wang, T. Regier, H. Dai, *Nat. Mater.*, 10(2011)780.
28. K. Deori, S. K. Ujjain, R. K. Sharma, S. Deka, *ACS Appl. Mater. Interfaces*, 5(2013)10665.
29. Q. Guan, J. Cheng, B. Wang, W. Ni, G. Gu, X. Li, L. Huang, G. Yang, F. Nie, *ACS Appl. Mater. Interfaces*, 6(2014)7626.
30. Y. Wang, Y. Lei, J. Li, L. Gu, H. Yuan, D. Xiao, *ACS Appl. Mater. Interfaces*, 6(2014)6739.
31. H. Xu, M. Shi, C. Liang, S. Wang, C. Xia, C. Xue, Z. Hai, S. Zhuiykov, *Nanoscale Res. Let.*, 13(2018)195.
32. J. Xie, H. Cao, H. Jiang, Y. Chen, W. Shi, H. Zheng, Y. Huang, *Anal. Chim. Acta*, 796(2013)92.
33. T. Meng, Q.-Q Xu, Z.-H. Wang, Y.-T. Li, Z.-M. Gao, X.-Y. Xing, T.-Z. Ren, *Electrochim. Acta*, 180(2015)104.
34. Z.-W. Fu, Y. Wang, Y. Zhang, Q. -Z. Qin, *Solid State Ionics*, 170(2004)105.
35. J. Yan, T. Wei, W. Qiao, B. Shao, Q. Zhao, L. Zhang, Z. Fan, *Electrochim. Acta*, 55(2010)6973.
36. J. Zhang, P. Tang, T. Liu, Y. Feng, C. Blackman, D. Li, *J. Mater. Chem. A*, 5(2017) 10387.
37. Y. Lu, L. Li, D. Chen, G. Shen, *J. Mater. Chem. A*, 5(2017)24981.
38. Z. Shang, M. Sun, S. Chang, X. Che, X. Cao, L. Wang, Y. Guo, W. Zhan, Y. Guo, G. Lu, *Appl. Catal., B*, 209(2017)33.
39. Y. Chen, Y. Li, Z. Hai, Y. Li, S. Kan, J. Chen, X. Chen, S. Zhuiykov, D. Cui, C. Xue, *Appl. Surf. Sci.*, 452(2018)413.
40. Y. Li, Z. Hai, X. Hou, H. Xu, Z. Zhang, D. Cui, C. Xue, B. Zhang, *J.Nanomater.*, (2017)1404328.
41. Y. Wang, Y. Lei, J. Li, L. Gu, H. Yuan, D. Xiao, *ACS Appl. Mater. Interfaces*, 6(2014)6739.
42. T. Li, S. Li, B. Zhang, B. Wang, D. Nie, Z. Chen, Y. Yan, N. Wan, W. Zhang, *Nanoscale Res. Lett.*, 10(2015)1.
43. S. Abouali, M. Akbari Garakani, B. Zhang, Z.-L. Xu, E. Kamali Heidari, J. Huang, J. Huang, J.-K. Kim, *ACS Appl. Mater. Interfaces*, 7(2015)13503.
44. H. Wang, Y. Shi, Z. Li, W. Zhang, S. Yao, *Chem. Res. Chin. Univ.*, 30(2014)650.
45. C. Yuan, L. Zhang, L. Hou, G. Pang, W.-C. Oh, *RSC Adv.*, 4(2014)14408.
46. D. Cai, H. Huang, D. Wang, B. Liu, L. Wang, Y. Liu, Q. Li, T. Wang, *ACS Appl. Mater. Interfaces*, 6(2014)15905.
47. R. Tummala, R. K. Guduru, P. S. Mohanty, *J. Power Sources*, 209(2012)44.
48. W. Zhou, J. Liu, T. Chen, K. S. Tan, X. Jia, Z. Luo, C. Cong, H. Yang, C. M. Li, T. Yu, *Phys. Chem. Chem. Phys.*, 13(2011)14462.
49. T. Zhu, J. S. Chen, X. W. Lou, *J. Mater. Chem.*, 20(2010)7015.
50. S. G. Kandalkar, H. -M. Lee, H. Chae, C.-K Kim, *Mater. Res. Bull.*, 46(2011)48.
51. W. Liu, D. Jiang, J. X. Xia, J. Qian, K. Wang, H. M. Li, *Monatsh. Chem.*, 145(2014)19.
52. M. Gao, W.-K Wang, Q. Rong, J. Jiang, Y.-J Zhang, H.-Q Yu, *ACS Appl. Mater. Interfaces*, 10(2018) 23163.
53. Y. Zhou, Y. Wang, J. Wang, L. Lin, X. Wu, D. He, *Mater. Lett.*, 216(2018)248.
54. D. Yu, J. Yao, L. Qiu, Y. Wang, X. Zhang, Y. Feng, H. Wang, *J. Mater. Chem. A*, 2(2014)8465.

55. P. Sennu, V. Aravindan, Y.S. Lee, *J. Power Sources*, 306(2016)248.